Multi-Target Location and Doppler Estimation in Multistatic Automotive Radar Applications

Ali Moussa, Wei Liu, Yimin D. Zhang, and Maria S. Greco

***Abstract*—In this paper, we develop a multistatic automotive radar scheme for enhanced localization and Doppler estimation of multiple targets exploiting cooperative roadside sensors. As the range between a target and a sensing vehicle cannot be directly measured, intermediate calculations are required to convert the measured bistatic range to the radial range of the targets of interest. Using the Fourier transform, the range resolution is thereby limited by the Rayleigh criterion applied to the total bistatic range. Developing a sparse representation for the bistatic automotive scenario can not only bypass the intermediate calculation step, but also add super-resolution sensing capability beyond the Rayleigh limit. As this application can benefit from the communication capabilities of the fifth-generation (5G) new radio (NR), multiple cooperative roadside transmitters are employed along a smart highway, forming a multistatic configuration. In order to process multiple realisations of the reflected signals simultaneously, we propose a solution employing the concept of group sparsity. Then, we show through computer simulations that, for some added complexity, better positioning performance can be achieved when compared to the state-of-art.**

***Index Terms*—automotive radar, multistatic, radar signal processing, sparse representation, location and Doppler estimation, group sparsity.**

I. Introduction

Radar-based sensing is a key enabling technology for autonomous driving and future intelligent transportation systems [1]–[4]. Recently, the automotive industry has benefited significantly from the development of various millimetre wave radar technologies deployed for applications such as adaptive cruise control, lane-change assistance, parking assistance, autonomous emergency brake, and advanced driver assistance systems (ADAS) [5]–[7]. A bistatic radar relies on a transmitter typically located far away from the receiver, and requires an additional reference receiver for collecting a direct-path signal needed as a reference for the demodulation task [8], [9]. Without loss of generality, any form of communication between the transmitter and the receiver that allows instantaneous sharing of the modulation parameters of the transmitted waveform, as well as tight time synchronisation, is sufficient for the operation of such radar systems.

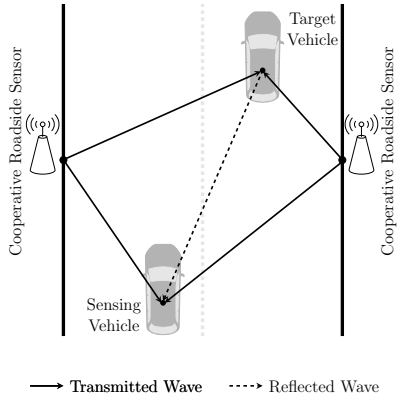

Figure 1. Multistatic automotive localisation scenario using two cooperative roadside sensors.

The interests to bistatic and multistatic radars resurged in the 1990s with more research drawn into statistical multiple-input multiple-output (MIMO) radar, bistatic synthetic-aperture-radar (SAR), remote sensing, and stealthy detection [10]–[14]. Bistatic and multistatic radars are also the foundation of passive radar systems as a means of green sensing technology [15], [16]. However, bistatic radar has since then struggled to break into the automotive industry, partly due to the very strict synchronisation requirements (in the order of nanoseconds [17]). Nonetheless, motivated by the drive in the fifth-generation (5G) communications and beyond to meet the requirements of vehicular applications [18], [19], as well as some advances in experimental radar synchronisation [20]–[22], automotive bistatic applications have been recently proposed to offer joint communication and radar capability for vehicles transmitting known communication modulation waveforms [23], enhanced detection in smart highway scenarios using cooperative roadside sensors transmitting radar signals [24], [25], and improved radar performance for vehicles exploiting a superposition of their monostatic measurements and bistatic ones from other road users [26]. At the same time, there are potential problems with such applications when employing Fourier techniques for localisation.

In this paper, a further extension to [24] is proposed where multiple cooperative roadside sensors are considered, resulting in a configuration known as multistatic (see Fig. 1). Our focus is on the two-dimensional (2D) localisation problem where the

A. Moussa is with the Department of Electronic and Electrical Engineering, University of Sheffield, UK.

W. Liu is with the School of Electronic Engineering and Computer Science, Queen Marry University of London, UK. His work is supported by the UK Engineering and Physical Sciences Research Council under grant EP/V009419/2. For the purpose of open access, the author has applied a Creative Commons Attribution (CC BY) licence to any Author Accepted Manuscript version arising.

Y. D. Zhang is with the Department of Electrical and Computer Engineering, Temple University, USA. His work was supported in part by the National Science Foundation (NSF) under grant No. ECCS-2236023.

M. S. Greco is with the Department of Ingegneria dell'Informazione, University of Pisa, Italy. Her work is partially supported by the Italian Ministry of Education and Research (MUR) in the framework of the FoReLab project (Departments of Excellence).

target range and direction-of-arrival (DOA) are simultaneously estimated followed by Doppler estimation for multiple targets. We refer to this problem as three-dimensional (3D) motion parameter estimation. Although the high efficiency of 3D fast Fourier transform (FFT) [27] and its good performance make it a straightforward candidate for extracting frequency information from an accumulation of signals corrupted by white noise [28], when multiple roadside sensors are in operation, it becomes difficult using FFT to coherently integrate range and Doppler measurements from different transmitter-receiver pairs [29]. To overcome this issue, more advanced signal processing techniques are needed, allowing processing information from multiple bistatic transmitter-receiver pairs on the data level.

While it is generally accepted that advanced signal processing techniques carry the extra computational cost, this consensus is destined to vanish as processing power retains its increasing trend. As a result, advanced signal processing techniques such as MUltiple SIgnal Classification (MUSIC) [30] and sparsity-based methods under the compressive sensing (CS) framework [31] have been hot topics in radar-related research in the last few decades [7], [32]–[34]. A sparse representation means that the signal can be modelled as a vector of finite/infinite parameters where only a few entries are non-zero; a set containing the indices of the non-zero entries in this sparse vector is known as the support. Researchers have adopted sparse representation from the CS framework and developed radar signal models for the DOA estimation problem [35]–[38] that can naturally be solved by popular techniques such as group LASSO [39], [40], also known as $\ell_{2,1}$ minimisation, and multistatic Bayesian sparse learning [41]–[43]. In particular, the structured sparsity problem arises when multiple sources of information share a common support set under the generally accepted narrowband assumption. Therefore, it naturally exists in radar applications, for instance, when multiple pulses, transmitters, or receivers are employed.

In this paper, we show that the extra degrees of freedom (DoFs) offered by prior information and multiple transmitters can be directly exploited following a sparse representation. We map the road as a Cartesian grid and enforce sparsity for simultaneous 2D localisation in a similar way as in [44], followed by Doppler estimation. With this approach, we avoid an exhaustive 3D parameter search, thereby significantly reducing the computational complexity. In order to pair the estimated location and Doppler parameters for each target, we propose two data association methods with varying performance and computational complexity. By performing extensive computer simulations, we convey the feasibility and superiority of the proposed sparsity-based positioning solutions in multistatic automotive configurations, and prove the success of the proposed data association methods under different settings.

Notations used in this work are as follows. Vectors and matrices are represented as lowercase and uppercase bold-face letters, respectively. $\{.\}^*$, $\{.\}^T$, and $\{.\}^H$ denote the complex conjugate, transpose, and Hermitian transpose of a vector or matrix, respectively. $\circ$, $\otimes$, and $\odot$ denote the outer product, the Kronecker product, and the element-wise (Hadammard) multiplication, respectively. diag$\{.\}$ returns a diagonal matrix,

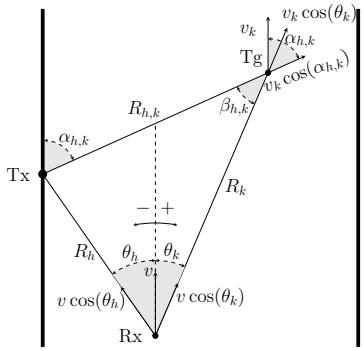

Figure 2. Geometry of the localisation problem.

vec$\{.\}$ is the vectorisation operation, and $E\{.\}$ is the expectation. $\|.\|_1$, $\|.\|_2$ and $\|.\|_F$ are the ℓ_1-norm, ℓ_2-norm and the Frobenius norm, respectively. The range parameters and Cartesian coordinates are in metres (m), velocity parameters in metres per second (m/s), and DOA/angle parameters in degrees ($^\circ$).

In the rest of this paper, a 3D multistatic frequency-modulated continuous-wave (FMCW) signal model is derived in Section II. Then, a multi-target location and Doppler estimation solution employing the group-sparsity (GS) concept in multistatic automotive configuration is proposed in Section III. Finally, simulation results are presented in Section IV, and conclusions are drawn in Section V.

II. 3D Multistatic FMCW Signal Model

Consider H stationary roadside sensors, each transmitting a frame of M narrowband FMCW chirps, with chirp repetition interval T and transmission duration per chirp equal to T_c. In reality, some form of orthogonality is introduced between the signals from different sensors to allow separating them at the receiver end [45], so we assume that the H sensors perform orthogonal transmissions in an appropriate domain. A single sensing vehicle is considered with K point targets present in the visible region of its radar module. Therefore, a single normalised transmitted chirp can be represented in the complex form as

$$s_0(t) = \begin{cases} e^{j2\pi\left[f_0 t + 0.5\mu t^2\right]} & t \in [0, T_c), \\ 0 & \text{otherwise}, \end{cases} \tag{1}$$

where f_0 denotes the starting frequency, t is the continuous real time, $\mu = \frac{B}{T_c}$ the modulation rate, and B the modulation bandwidth. Then, the transmitted normalised frame can be represented as

$$s_M(t) = \sum_{m=0}^{M-1} s_0(t - mT). \tag{2}$$

Since the signal $s_M(t)$ is periodic, time t can be decomposed into fast time t_f and slow time mT such that

$$t = t_f + mT, \quad t_f \in [0, T_c). \tag{3}$$

Accordingly,

$$s_0(t) = s_0(t_f + mT) = s_0(t_f). \tag{4}$$

While $s_M(t)$ is a superposition of M chirps, it is convenient with the proposed decomposition of time to represent the normalised transmitted signal for the m-th chirp at time t_f as

$$s(m, t_f) = s_0(t_f). \tag{5}$$

Without loss of generality, we assume that all vehicles are moving forward along the direction of the lane with a constant velocity over the considered period of signal transmission such that the sensing vehicle drives towards the roadside sensor with velocity v and target vehicle drives away from it with velocity v_k. In the sequel, the subscripts k and h denote any parameters or signals corresponding to the k-th target and the h-th roadside sensor, respectively, and h, k denotes any combination of both, where $k = 1, 2, \ldots, K$ and $h = 1, 2, \ldots, H$.

As depicted in Fig. 2, the velocity of the sensing vehicle with respect to the h-th roadside sensor can be defined as

$$v_h = v \cos(\theta_h), \tag{6}$$

where θ_h is the DOA of the h-th roadside sensor observed from the sensing vehicle. Similarly, the velocity projected on each path of the bistatic target signal is the bistatic velocity and can be defined as

$$v_{h,k} = v_k \left[\cos(\alpha_{h,k}) + \cos(\theta_k)\right] - v \cos(\theta_k), \tag{7}$$

where

$$\alpha_{h,k} = \begin{cases} \arcsin\left(\frac{R_h}{R_{h,k}} \sin(|\theta_h - \theta_k|)\right) + \theta_k, & \text{for} \quad \theta_h \leq 0°, \\ \arcsin\left(\frac{R_h}{R_{h,k}} \sin(|\theta_h - \theta_k|)\right) - \theta_k, & \text{for} \quad \theta_h \geq 0°, \end{cases} \tag{8}$$

θ_k is the DOA of the k-th target vehicle, R_h is the range between the h-th roadside sensor and the sensing vehicle (also known as the baseline), and $R_{h,k}$ is the range between the h-th roadside sensor and the k-th target vehicle and can be defined as

$$R_{h,k} = \acute{R}_{h,k} - R_k, \tag{9}$$

with R_k being the range between of the k-th target and the sensing vehicle, and $\acute{R}_{h,k}$ is the bistatic range.

Suppose that the sensing vehicle is equipped with a uniform linear array (ULA) of L antennas with adjacent sensor spacing d [46]. By following a free-space path-loss model, the direct-path signal received at the l-th antenna of the sensing vehicle corresponding to the h-th roadside sensor and can be expressed as

$$r_h(l, m, t_f) = A_h s_0(t_f - \tau_h(m, t_f)) e^{-j2\pi\phi_h(l)}, \tag{10}$$

with

$$\tau_h(m, t_f) = \frac{R_h}{c} + \frac{v_h}{c}(t_f + mT), \tag{11}$$

where τ_h denotes the time delay of the direct-path signal, $\phi_h(l) = \frac{f_0 d \sin\theta_h}{c} l$ is the phase delay relative to the 0-th antenna of the sensing vehicle array with $l = 0, 1, \ldots, L-1$ being the antenna index, c is the wave propagation speed, and $A_h = \sqrt{\frac{P_t G_t G_r c^2}{(4\pi)^2 f_0^2 R_h^2}}$ is the amplitude of the received direct-path signal with P_t being the transmitted power, and G_t and G_r are the transmitter and receiver antenna gains, respectively.

Similarly, a bistatic signal reflected from the k-th target and received at the sensing vehicle can be expressed as

$$r_{h,k}(l, m, t_f) = A_{h,k} s_0(t_f - \tau_{h,k}(m, t_f)) e^{-j2\pi\phi_k(l)}, \tag{12}$$

with

$$\tau_{h,k}(m, t_f) = \frac{\acute{R}_{h,k}}{c} + \frac{v_{h,k}}{c}(t_f + mT), \tag{13}$$

where $\tau_{h,k}$ denotes the time delay of the bistatic target signal, $\phi_k(l) = \frac{f_0 d \sin\theta_k}{c} l$ is the phase delay relative to the 0-th antenna, and $A_{h,k} = \sqrt{\frac{P_t G_t G_r \sigma c^2}{(4\pi)^3 f_0^2 R_k^2 R_{h,k}^2}}$ is the amplitude of the received target signal with σ being the radar cross-section (RCS). We assume here, for the sake of simplicity, that σ is constant and equal for all considered targets, and the received signal amplitude is deterministic.

To extract the embedded information, the received signal is cross-correlated with a signal identical to the one in (1) generated locally. We assume perfect synchronisation with the modulation settings already known. Further, we assume that the location of the roadside sensor (R_h, θ_h) is known and that the signal r_h has already been removed at the receiver. Note that knowledge of the roadside sensor location allows us to more effectively remove the direct-path signal as explained below:

1) The peak corresponding to the direct-path signal can be unambiguously identified since $\tau_h < \tau_{h,k}$ (triangle inequality in Fig. 2 with $R_h < (R_{h,k} + R_k)$) and the intensity of the peak is strictly higher than the ones corresponding to bistatic reflections.
2) The Global Positioning System (GPS) coordinates of the roadside sensor can be accessed by the sensing vehicle through the established new radio (NR) communication link. With access to its own GPS coordinates, the sensing vehicle can then implement data fusion to better estimate the direct-path signal (Note that the availability of accurate GPS coordinates is not necessary for the feasibility of this application but can help optimise the estimation and the removal of the direct-path signals).
3) Direct-path removal techniques have been studied extensively in the literature, and the feasibility of such task has already been proven [47]–[49]. Moreover, having access to two sources of information related to the direct-path signal (through radar processing and NR communications) can intuitively improve the performance of those techniques.

Therefore, in the presence of K targets and assuming that the direct-path signal is removed, the resultant beat signal (also known as the intermediate frequency (IF) signal) corresponding to the h-th sensor can be modelled in line with that in [50]. The dechirped signal can then be written as

$$\begin{aligned} &y_h(l, m, t_f) \\ &= \sum_{k=1}^{K} A_{h,k} e^{-j2\pi\left[\frac{f_0 \acute{R}_{h,k}}{c} + \frac{\mu \acute{R}_{h,k}}{c} t_f + \frac{f_0 v_{h,k}}{c} mT\right]} e^{-j2\pi\phi_k(l)} \\ &\quad + w_h(l, m, t_f), \end{aligned} \tag{14}$$

where w_h is the additive white Gaussian noise (AWGN). The dechirped signal is sampled at a rate f_s such that

$n = 0, 1, \ldots, N-1$ is the sampling index and $N = f_s T_c$ is the total number of fast-time samples, also known as snapshots. It can then be written as a function of antenna index l, slow-time index m, and fast-time index n as

$$\hat{y}_h[l,m,n] = \sum_{k=1}^{K} q_{h,k} e^{-j2\pi\left[\frac{\mu \acute{R}_{h,k}}{c}\frac{n}{f_s} + \frac{f_0 v_{h,k}}{c} mT + \frac{f_0 d \sin\theta_k}{c} l\right]} + \hat{w}_h[l,m,n], \tag{15}$$

where $q_{h,k} = A_{h,k} e^{-j2\pi \frac{f_0 \acute{R}_{h,k}}{c}}$.

The results in (15) can be structured to form a tensor $\boldsymbol{\mathcal{Y}}_h \in \mathbb{C}^{L\times M\times N}$ such that

$$\boldsymbol{\mathcal{Y}}_h = \sum_{k=1}^{K} q_{h,k}(\mathbf{a}_k \circ \mathbf{v}_{h,k} \circ \mathbf{r}_{h,k}) + \boldsymbol{\mathcal{W}}_h, \tag{16}$$

where $\boldsymbol{\mathcal{W}}_h \in \mathbb{C}^{L\times M\times N}$ is the AWGN tensor,

$$\mathbf{a}_k = \left[1, e^{-j2\pi \frac{f_0 d \sin\theta_k}{c}}, \ldots, e^{-j2\pi \frac{f_0 d \sin\theta_k}{c}(L-1)}\right]^T \tag{17}$$

is an $L \times 1$ column vector representing the array steering vector,

$$\mathbf{v}_{h,k} = \left[1, e^{-j2\pi \frac{f_0 v_{h,k}}{c} T}, \ldots, e^{-j2\pi \frac{f_0 v_{h,k}}{c}(M-1)T}\right]^T \tag{18}$$

is an $M \times 1$ column vector representing the Doppler steering vector, and

$$\mathbf{r}_{h,k} = \left[1, e^{-j2\pi \frac{\mu \acute{R}_{h,k}}{c}\frac{1}{f_s}}, \ldots, e^{-j2\pi \frac{\mu \acute{R}_{h,k}}{c}\frac{N-1}{f_s}}\right]^T \tag{19}$$

is an $N \times 1$ column vector representing the range steering vector.

Next, the antenna and fast-time domains are stacked together against the slow time, and the tensor $\boldsymbol{\mathcal{Y}}_h$ can be reshaped into a matrix $\mathbf{Y}_h \in \mathbb{C}^{LN\times M}$ such that

$$\mathbf{Y}_h = \sum_{k=1}^{K} q_{h,k}\left(\mathbf{p}_{h,k}\mathbf{v}_{h,k}^T\right) + \mathbf{W}_h, \tag{20}$$

where $\mathbf{p}_{h,k} = \mathbf{r}_{h,k} \otimes \mathbf{a}_k$ and $\mathbf{W}_h \in \mathbb{C}^{LN\times M}$ is the AWGN matrix.

Finally, $\mathbf{Y}_h$ can be written in a more compact format as

$$\mathbf{Y}_h = \mathbf{P}_h \mathbf{X}_h \mathbf{V}_h^T + \mathbf{W}_h, \tag{21}$$

where $\mathbf{P}_h = [\mathbf{p}_{h,1}, \mathbf{p}_{h,2}, \ldots, \mathbf{p}_{h,K}] \in \mathbb{C}^{LN\times K}$ contains the range-DOA information, $\mathbf{V}_h = [\mathbf{v}_{h,1}, \mathbf{v}_{h,2}, \ldots, \mathbf{v}_{h,K}] \in \mathbb{C}^{M\times K}$ contains the Doppler information, and $\mathbf{X}_h = \text{diag}\{q_{h,1}, q_{h,2}, \ldots, q_{h,K}\} \in \mathbb{C}^{K\times K}$ contains the complex amplitude.

Let $(R,\theta)_k := (R_k, \theta_k)$ and $(R,\theta)_h := (R_h, \theta_h)$. Following the earlier assumption, the parameters $(R,\theta)_h$ are known to the sensing vehicle. By exploiting this and using the geometry depicted in Fig. 2, $\acute{R}_{h,k}$ can be obtained as

$$\acute{R}_{h,k} = \sqrt{R_k^2 + R_h^2 - 2R_k R_h \cos(\theta_h - \theta_k)} + R_k. \tag{22}$$

The aim is to estimate $(R,\theta)_k$ and v_k. After applying 3D FFT to (16), the spectrum would show K peaks corresponding to $(\acute{R}_{h,k}, \theta_k, v_{h,k})$ for all k. Using (22), R_k can be calculated as

$$R_k = \frac{\acute{R}_{h,k}^2 - R_h^2}{2\acute{R}_{h,k} - 2R_h\cos(\theta_h - \theta_k)}. \tag{23}$$

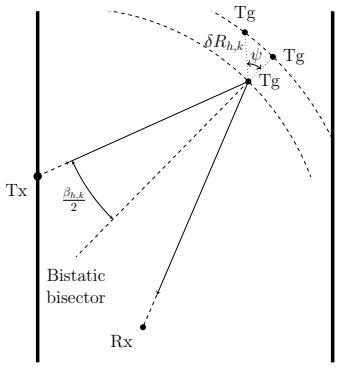

Figure 3. Bistatic range resolution.

The generalised bistatic range resolution can be defined as [17]

$$\delta R_{h,k}(\psi) = \frac{c}{2B\cos(\beta_{h,k}/2)\cos\psi}, \tag{24}$$

where $\beta_{h,k}$ is the bistatic angle (shown in Fig. 2) and ψ is the rotation angle from the bistatic bisector as shown in Fig. 3.

After R_k and θ_k are estimated, using (7) and (8) and assuming known v, v_k can be estimated as

$$v_k = \frac{v_{h,k} + v\cos(\theta_k)}{\cos(\alpha_{h,k}) + \cos(\theta_k)}. \tag{25}$$

Remark. *In bistatic radar, the range resolution varies in 2D depending on the geometry. Therefore, it can no longer be defined in one specific direction (such as down-range in the monostatic case). In* (24)*, the direction of range resolution is dictated by the rotation angle ψ away from the bistatic bisector which is considered as the reference point (see Fig. 3 for an illustration of three possible placements of targets). Clearly, the down-range resolution is maximum when $\psi = 0°$, and as one target rotates away from the bisector ($\psi > 0°$), the resolution is degraded. When $\psi = 90°$, the two considered targets lie on the same iso-range contour and can no longer be resolved in the range domain.*

On the other hand, $\beta_{h,k}$ determines the effect of the bistatic geometry on the overall range resolution regardless of the direction of interest. Clearly, when $\beta_{h,k} = 0°$, the bistatic range resolution is maximised and reduces to the monostatic one. It is important to note here that, for a given target, the range resolution varies with the location of the h-th roadside sensor. This highlights the advantage of multistatic configuration in increasing the number of DoFs when signal processing techniques permit fusion at the data level. In the case of Fourier-based estimation, although two targets that cannot be resolved in the range domain may still be resolved in the range-DOA 2D FFT spectra, the conversion in (23) *to calculate the range R_k introduces some bias imposed by the estimate of θ_k. Similarly, the conversion in* (25) *to calculate the velocity v_k introduces some bias imposed by the estimates of R_k and θ_k.*

Some further problems emerge when using Fourier-based estimation in this application. The first problem occurs when some information is known *a priori*, since the FFT fails to

integrate such information directly and can only be done in post-processing steps. The second problem naturally arises in the multistatic configuration because the FFT cannot be applied across the domain created by the multiple roadside sensors. In other words, the FFT cannot be applied across the signals received from H roadside sensors in a similar manner to the signals received at L antennas, for instance, since there is no correlation between the H signals. This limits the benefit of integration gain to the domain corresponding to the parameter being estimated [46]. It follows that the fusion of multistatic signals in the FFT domain may only be done post-calculation rather than at the measurement level. Furthermore, suppose there exist H independent FFT spectra from which R_k is estimated. The final estimate after averaging can be expressed as

$$\bar{R}_k = R_k + \bar{\epsilon}, \tag{26}$$

such that

$$\bar{\epsilon} = \frac{1}{H}\sum_{h=1}^{H} \epsilon_h, \tag{27}$$

where ϵ_h denotes the bias of the calculated range from the h-th source of information. When ϵ_h follows a Gaussian distribution $\mathcal{N}(\bar{\mu}, \sigma_a^2)$ with $\bar{\mu}$ and σ_a^2 being the mean and variance, respectively, then $\bar{\epsilon}$ follows $\mathcal{N}(\bar{\mu}, \sigma_a^2/H)$. In this case, averaging the estimates only reduces the error variance by a factor of H, but does not affect the shape of the probability density function (PDF). This analysis also applies to the averaging estimates of v_k. For DOA estimation, one may argue that the DOA-FFT spectra can be averaged directly because all H signals share the same frequencies corresponding to θ_k. However, such an approach, often known as incoherent integration, may only reduce the variance of the estimated noise floor, meaning that the average noise power level remains unchanged.

III. Proposed Multistatic Localisation and Doppler Estimation Using GS in Multi-target Automotive Scenario

A. Sparse Representation for Multistatic Cartesian 2D Localisation

One DoF associated with the representation in (21) is the ability to design the steering matrix to incorporate $(R,\theta)_h$ known prior to estimation. Therefore, a 2D polar grid of length G_p is defined to search for range and DOA $(R,\theta)_{g_p} := (R_{g_p}, \theta_{g_p})$ to simultaneously estimate $(R,\theta)_k$. Then, for each roadside sensor, an overcomplete range-DOA steering matrix $\mathbf{P}_{\mathbf{g},h} \in \mathbb{C}^{LN\times G_p}$ is constructed with its g_p-th column given as $\mathbf{p}_{h,g_p} = \tilde{\mathbf{r}}_{h,g_p} \otimes \mathbf{a}_{g_p}$, where

$$\mathbf{a}_{g_p} = \left[1, e^{-j2\pi\frac{f_0 d\sin\theta_{g_p}}{c}}, \ldots, e^{-j2\pi\frac{f_0 d\sin\theta_{g_p}}{c}(L-1)}\right]^T \tag{28}$$

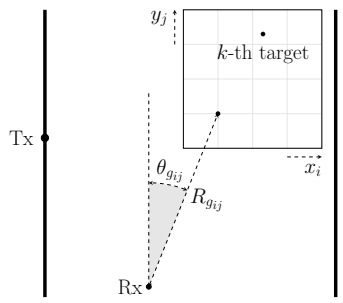

Figure 4. Proposed 2D rectangular search grid.

and

$$\tilde{\mathbf{r}}_{h,g_p} = \begin{bmatrix} 1 \\ e^{-j2\pi\left[\left(\mu\sqrt{R_{g_p}^2+R_h^2-2R_{g_p}R_h\cos(\theta_h-\theta_{g_p})}+R_{g_p}\right)\frac{1}{cf_s}\right]} \\ \vdots \\ e^{-j2\pi\left[\left(\mu\sqrt{R_{g_p}^2+R_h^2-2R_{g_p}R_h\cos(\theta_h-\theta_{g_p})}+R_{g_p}\right)\frac{N-1}{cf_s}\right]} \end{bmatrix}. \tag{29}$$

Then, (21) can be written in a standard sparse format as

$$\mathbf{Y}_h^{\mathbf{P}} = \mathbf{P}_{\mathbf{g},h}\mathbf{X}_{\mathbf{g},h}^{\mathbf{P}} + \mathbf{W}_h, \tag{30}$$

where $\mathbf{X}_{\mathbf{g},h}^{\mathbf{P}} \in \mathbb{C}^{G_p\times M}$ is a sparse data matrix whose m-th column contains K non-zero entries corresponding to the complex coefficients of target echoes from the h-th transmitted signal. We assume that all columns have the exact support set containing the indices of the non-zero entries.

This road scenario motivates the idea of constructing a 2D rectangular search grid of size $I \times J$ and coordinates (x_i, y_j) with $i = 1, 2, \ldots, I$ and $j = 1, 2, \ldots, J$ as shown in Fig. 4. By taking the sensing vehicle as the centre of the Cartesian map, it is clear that y_j is always positive whereas the sign of x_i mirrors θ_{g_p} with the forward line being the reference. Following this, g_p is now replaced with g_{ij} which corresponds to the ij-th bin in the 2D rectangular grid.

Next, the g_{ij}-th column in $\mathbf{P}_{\mathbf{g},h}$ can be constructed by converting the ij-th Cartesian coordinates (x_i, y_j) into polar coordinates $(R,\theta)_{g_{ij}} := (R_{g_{ij}}, \theta_{g_{ij}})$ as

$$(R,\theta)_{g_{ij}} = \left(\sqrt{x_i^2+y_j^2}, \arcsin\left(\frac{x_i}{\sqrt{x_i^2+y_j^2}}\right)\right). \tag{31}$$

Accordingly, the Cartesian coordinates of the k-th target can be defined as

$$(x,y)_k = (R_k\sin\theta_k, R_k\cos\theta_k) \tag{32}$$

and do not necessarily lie on an exact coordinate of the generated rectangular search grid.

B. Sparse Representation for Multistatic Doppler Estimation

The raw data in (21) is reshaped to get

$$\mathbf{Z}_h = \mathbf{Y}_h^T. \tag{33}$$

A velocity grid of length G_d is defined to search for v_{h,g_d} to estimate $v_{h,k}$. Then, an overcomplete Doppler steering matrix

$\mathbf{V}_{\mathbf{g},h} \in \mathbb{C}^{M\times G_d}$ is constructed by replacing $v_{h,k}$ with v_{h,g_d} in $\mathbf{V}_h$ such that

$$v_{h,g_d} \in \left[v_{\min,h}, v_{\max,h}\right], \tag{34}$$

where

$$\begin{aligned} v_{\min,h} &= \min\left\{v_{\min}[\cos(\alpha_{h,g_{ij}}) + \cos(\theta_k)] - v\cos(\theta_k)\right\}, \\ v_{\max,h} &= \min\left\{v_{\max}[\cos(\alpha_{h,g_{ij}}) + \cos(\theta_k)] - v\cos(\theta_k)\right\}, \end{aligned}$$

$$\alpha_{h,g_{ij}} = \begin{cases} \arcsin\left(\frac{R_h \sin(|\theta_h - \theta_{g_{ij}}|)}{\sqrt{R_{g_{ij}}^2 + R_h^2 - 2R_{g_{ij}}R_h\cos(\theta_h - \theta_{g_{ij}})}}\right) \\ \qquad\qquad +\theta_{g_{ij}}, \quad \text{for} \quad \theta_h \le 0^\circ, \\ \arcsin\left(\frac{R_h \sin(|\theta_h - \theta_{g_{ij}}|)}{\sqrt{R_{g_{ij}}^2 + R_h^2 - 2R_{g_{ij}}R_h\cos(\theta_h - \theta_{g_{ij}})}}\right) \\ \qquad\qquad -\theta_{g_{ij}}, \quad \text{for} \quad \theta_h \ge 0^\circ, \end{cases} \tag{35}$$

and $v_{\min}$ and $v_{\max}$ denote the minimum and maximum values of the potential forward velocities of the target, respectively. Accordingly, $\mathbf{Z}_h$ can now be written in a standard sparse format as

$$\mathbf{Z}_h^{\mathbf{D}} = \mathbf{V}_{\mathbf{g},h}\mathbf{X}_{\mathbf{g},h}^{\mathbf{D}} + \mathbf{W}_h^T, \tag{36}$$

where $\mathbf{X}_{\mathbf{g},h}^{\mathbf{D}} \in \mathbb{C}^{G_d\times LN}$ is a sparse data matrix whose $(lN+n)$-th column contains K non-zero entries corresponding to the complex coefficients of the visible targets and have the same support set.

C. Multistatic Localisation and Doppler Estimation Using GS

Firstly, the 2D location denoted by $(x,y)_k$ is to be estimated through reconstructing $\mathbf{X}_{\mathbf{g},h}^{\mathbf{P}}$ from $\mathbf{Y}_h$. All columns in the H matrices $\mathbf{X}_{\mathbf{g},h}^{\mathbf{P}}$ have the same support set corresponding to K locations $(x,y)_k$. So, the concept of GS can be employed across M pulses and H sensors by generating an $LN \times MH$ measurement matrix $\mathbf{B}_{\mathbf{g}}^{\mathbf{P}}$ and a $G_p \times MH$ sparse data matrix $\mathbf{U}_{\mathbf{g}}^{\mathbf{P}}$ as

$$\mathbf{B}_{\mathbf{g}}^{\mathbf{P}} = \left[\mathbf{P}_{\mathbf{g},1}\mathbf{X}_{\mathbf{g},1}^{\mathbf{P}}, \mathbf{P}_{\mathbf{g},2}\mathbf{X}_{\mathbf{g},2}^{\mathbf{P}}, \ldots, \mathbf{P}_{\mathbf{g},H}\mathbf{X}_{\mathbf{g},H}^{\mathbf{P}}\right], \tag{37}$$

$$\mathbf{U}_{\mathbf{g}}^{\mathbf{P}} = \left[\mathbf{X}_{\mathbf{g},1}^{\mathbf{P}}, \mathbf{X}_{\mathbf{g},2}^{\mathbf{P}}, \ldots, \mathbf{X}_{\mathbf{g},H}^{\mathbf{P}}\right]. \tag{38}$$

Denote row vector $\mathbf{u}_{\mathbf{g},g_p}^{\mathbf{P}}$ as the g_p-th row of the matrix $\mathbf{U}_{\mathbf{g}}^{\mathbf{P}}$. By computing the ℓ_2 norm to each row vector $\mathbf{u}_{\mathbf{g},g_p}^{\mathbf{P}}$, a new column vector is formed as

$$\widetilde{\mathbf{u}}_{\mathbf{g}}^{\mathbf{P}} = \left[\|\mathbf{u}_{\mathbf{g},1}^{\mathbf{P}}\|_2, \|\mathbf{u}_{\mathbf{g},2}^{\mathbf{P}}\|_2, \ldots, \|\mathbf{u}_{\mathbf{g},G_p}^{\mathbf{P}}\|_2\right]^T. \tag{39}$$

Then, the GS-based multistatic localisation method is formulated as follows [51], [52]

$$\min_{\mathbf{U}_{\mathbf{g}}^{\mathbf{P}}} \quad \|\widetilde{\mathbf{u}}_{\mathbf{g}}^{\mathbf{P}}\|_1 \quad \text{subject to} \quad \|\mathbf{Y}^\circ - \mathbf{B}_{\mathbf{g}}^{\mathbf{P}}\|_F \le \varepsilon_1, \tag{40}$$

where

$$\mathbf{Y}^\circ = \left[\mathbf{Y}_1, \mathbf{Y}_2, \ldots, \mathbf{Y}_H\right], \tag{41}$$

and ε_1 is the reconstruction error.

Next, after estimating $(x,y)_k$, the bistatic velocity parameter denoted by $v_{h,k}$ is to be estimated through reconstructing $\mathbf{X}_{\mathbf{g},h}^{\mathbf{D}}$ from $\mathbf{Z}_h$. Notice that, while the columns in $\mathbf{X}_{\mathbf{g},h}^{\mathbf{D}}$ share the same support set, the latter varies across H Doppler data matrices. This is dictated by the steering matrix $\mathbf{V}_{\mathbf{g},h}$ that is designed to search for $v_{h,k}$ rather than v_k. Alternatively, the steering matrix could be designed to directly search for v_k. In such a case, all columns in the H data matrices would share the same support set corresponding to all K parameters. Although this approach may offer the advantage of employing the GS concept across H sensors as well as L antennas and N snapshots, it may suffer from ambiguities due to the coupling between velocity, range, and DOA in (7) and (8). To illustrate this, the search grid would have to be populated K times and, depending on the 2D locations of the targets, the estimated bistatic velocities may migrate to other values which do not necessarily correspond to their true velocities in the search grid. This is due to the fact that there is no mechanism in ℓ_1 norm to ensure either an even or an uneven distribution of sparsity among all K groups of the search grid. Ideally, sparsity can be enforced across all H sensors to estimate R_k, θ_k, and v_k simultaneously. However, this requires handling steering matrices of size $LMN \times G_dG_p$ which is computationally exhaustive.

For the h-th measurement matrix $\mathbf{Z}_h$, the GS concept can be employed across LN snapshots. Therefore, Doppler estimation is performed by solving the following optimisation problem

$$\min_{\mathbf{X}_{\mathbf{g},h}^{\mathbf{D}}} \quad \|\widetilde{\mathbf{x}}_{\mathbf{g},h}^{\mathbf{D}}\|_1 \quad \text{subject to} \quad \|\mathbf{Z}_h - \mathbf{V}_{\mathbf{g},h}\mathbf{X}_{\mathbf{g},h}^{\mathbf{D}}\|_F \le \varepsilon_2, \tag{42}$$

where

$$\widetilde{\mathbf{x}}_{\mathbf{g},h}^{\mathbf{D}} = \left[\|\mathbf{x}_{\mathbf{g},h,1}^{\mathbf{D}}\|_2, \|\mathbf{x}_{\mathbf{g},h,2}^{\mathbf{D}}\|_2, \ldots, \|\mathbf{x}_{\mathbf{g},h,G_d}^{\mathbf{D}}\|_2\right]^T, \tag{43}$$

$\mathbf{x}_{\mathbf{g},g_d}^{\mathbf{D}}$ is the g_d-th column of $\mathbf{X}_{\mathbf{g}}^{\mathbf{D}}$ and ε_2 is the reconstruction error. Both optimisation problems (40) and (42) are convex and can be solved using existing convex optimisation toolboxes. Finally, the proposed GS-based method for location and Doppler estimation of K targets in this multistatic automotive scenario is summarised in Algorithm 1.

D. Multi-target Parameter Association Using Cross-Correlation and ESPRIT

While the values of $(x,y)_k$ and $v_{h,k}$ can be estimated using Algorithm 1, the information regarding the association of the location with the corresponding bistatic velocity for each target remains unknown. Such pairing is essential for establishing a complete profile about the targets and for computing the velocity v_k using (25). So, motivated by the cross-correlation (CC)-based pair-matching method for elevation and azimuth in L-shaped antenna arrays [53], a modification is proposed here for matching the location and bistatic velocity pairs. Each 2D location corresponds to a unique angle θ_k, so the parameter association task renders a matching between the DOA and bistatic velocity parameters. This can be done by exploiting the CC matrix $\mathbf{R}_{\boldsymbol{\theta}\boldsymbol{v},h}$ which is defined as

$$\mathbf{R}_{\boldsymbol{\theta}\boldsymbol{v},h} = E\left\{\mathbf{y}_{\boldsymbol{\theta},h}(n)\mathbf{y}_{\boldsymbol{v},h}^H(n)\right\}, \tag{44}$$

where the l-th entry of $\mathbf{y}_{\boldsymbol{\theta},h}(n) \in \mathbb{C}^{L\times 1}$ is equal to $\hat{y}_h[l,0,n]$ in (15) and the m-th entry of $\mathbf{y}_{\boldsymbol{v},h}(n) \in \mathbb{C}^{M\times 1}$ is equal to $\hat{y}_h[0,m,n]$. Clearly, $\mathbf{R}_{\boldsymbol{\theta}\boldsymbol{v},h}$ can only be computed when $L = M$. Unlike the case in [53] where both received signals corresponding to the two components of the L-shaped array

Algorithm 1 A GS-based location and Doppler estimation algorithm for multistatic automotive application.

Require: $\mathbf{Y}_h$, R_h, θ_h, v, f_0, μ, d, T, M, L, f_s, N, H.

1: Obtain and store the raw data $\mathbf{Y}_h$ for all h as in (20).
2: Generate an $I \times J$ rectangular search grid of length G_p after choosing appropriate values for (x_1, y_1) and (x_I, y_J).
3: Convert the Cartesian coordinates (x_i, y_j) to polar coordinates $(R, \theta)_{g_{ij}}$ using (31).
4: For each roadside sensor, construct a range-DOA steering matrix $\mathbf{P}_{\mathbf{g},h}$ whose g_{ij}-th column corresponds to (x_i, y_j).
5: Estimate $\mathbf{U}_{\mathbf{g}}^{\mathbf{P}}$ by solving the optimisation problem (40).
6: Perform a peak search to find the estimated coordinates of K targets.
7: Reshape the raw data as in (33) to get $\mathbf{Z}_h$.
8: After selecting appropriate values of $v_{\min}$ and $v_{\max}$, using v and all G_p values of $(R, \theta)_{g_{ij}}$, calculate $v_{\min,h}$ and $v_{\max,h}$ for all h using (35).
9: Generate H velocity search grids of length G_d using (34).
10: For each roadside sensor, construct a Doppler steering matrix $\mathbf{V}_{\mathbf{g},h}$ whose g_d-th column corresponds to v_{h,g_d}.
11: Estimate $\mathbf{X}_{\mathbf{g},h}^{\mathbf{D}}$ by solving the optimisation problem (42) for all h.
12: Perform a peak search to find the estimated bistatic velocity values of K targets.
13: **return** Estimates of $(x, y)_k$ and $v_{h,k}$ for all K targets.

have the same length, L is smaller than M in the underlying problem. Therefore, only the first L entries of $\mathbf{y}_{\boldsymbol{v},h}(n)$ are considered, from which $\breve{\mathbf{y}}_{\boldsymbol{v},h}(n)$ is formed. Accordingly, $\mathbf{R}_{\boldsymbol{\theta v},h}$ becomes an $L \times L$ matrix whose diagonal elements lead to the following formulation

$$\mathbf{d}_{\boldsymbol{\theta v},h} = \left[\sum_{k=1}^{K} q_{h,k}, \sum_{k=1}^{K} q_{h,k} e^{-j\zeta\omega_{h,k}}, \ldots, \sum_{k=1}^{K} q_{h,k} e^{-j\zeta(L-1)\omega_{h,k}}\right]^T, \tag{45}$$

where $\zeta = 2\pi f_0/c$ and $\omega_{h,k} = d\sin\theta_k - TV_{h,k}$. Denote by $\hat{\mathbf{d}}_{\boldsymbol{\theta v},h}$, $\hat{\theta}_k$, $\hat{v}_{h,k}$, and $\hat{\omega}_{h,k}$ the estimated versions of $\mathbf{d}_{\boldsymbol{\theta v},h}$, θ_k, $v_{h,k}$, and $\omega_{h,k}$ respectively. Our implementation for the pairing method can then be summarised as follows.

1) Using the estimated values $\hat{\theta}_k$ and $\hat{v}_{h,k}$, calculate K^2 combinations of $\{d\sin\hat{\theta}_{k_\theta} - T\hat{v}_{h,k_v}\}$, where $k_\theta, k_v = 1, 2, \ldots, K$.
2) Obtain $\hat{\mathbf{d}}_{\boldsymbol{\theta v},h}$ from $\mathbf{y}_{\boldsymbol{\theta},h}$ and $\breve{\mathbf{y}}_{\boldsymbol{v},h}$ as

$$\hat{\mathbf{d}}_{\boldsymbol{\theta v},h} = \frac{1}{N}\sum_{n=1}^{N} \mathbf{y}_{\boldsymbol{\theta},h}(n) \odot \breve{\mathbf{y}}^*_{\boldsymbol{v},h}(n), \tag{46}$$

then construct a Hermitian Toeplitz matrix, $\hat{\mathbf{R}}_{\boldsymbol{cc},h}$, whose first column is $\hat{\mathbf{d}}_{\boldsymbol{\theta v},h}$.
3) Apply ESPRIT [54] to $\hat{\mathbf{R}}_{\boldsymbol{cc},h}$ to estimate $\omega_{h,k}$ for K targets.
4) For the k-th target, the correct combination of DOA and velocity parameters is determined by solving the following minimisation problem

$$\min_{k_\theta, k_v} \left| e^{-j\zeta\hat{\omega}_{h,k}} - e^{-j\zeta(d\sin\hat{\theta}_{k_\theta} - T\hat{v}_{h,k_v})} \right|. \tag{47}$$

Note that Step 4 above adopts the comments in [55] to expand the unambiguous parameter range of this pair matching method.

E. Multi-target Parameter Association based on Least Squares

Unlike the previous parameter association method, matching here is done between the estimated 2D locations and the bistatic velocity parameters. To illustrate this, consider the following reformulation of (21)

$$\mathbf{y}_h = \mathrm{vec}\{\mathbf{Y}_h\} = \mathbf{A}_h\mathbf{x}_h + \mathbf{w}_h, \tag{48}$$

where

$$\mathbf{A}_h = \left[(\mathbf{p}_{h,1} \otimes \mathbf{v}_{h,1}), (\mathbf{p}_{h,2} \otimes \mathbf{v}_{h,2}), \ldots, (\mathbf{p}_{h,K} \otimes \mathbf{v}_{h,K})\right], \tag{49}$$

$$\mathbf{x}_h = \left[q_{h,1}, q_{h,2}, \ldots, q_{h,K}\right]^T, \tag{50}$$

and $\mathbf{w}_h = \mathrm{vec}\{\mathbf{W}_h\}$. By focusing on $\mathbf{A}_h$ we can see that once $\mathbf{p}_{h,k}$ and $\mathbf{v}_{h,k}$ are constructed from the estimated location and bistatic velocity, the task becomes to find the combination that minimises the distance between the matrix $\mathbf{A}_h$ and its reconstruction. Thus, we propose the following least-squares (LS)-based minimisation problem

$$\min_{\hat{\mathbf{A}}_h} \left\| \mathbf{y}_h - \hat{\mathbf{A}}_h(\hat{\mathbf{A}}_h^H\hat{\mathbf{A}}_h)^{-1}\hat{\mathbf{A}}_h^H\mathbf{y}_h \right\|_2, \tag{51}$$

where $\hat{\mathbf{A}}_h$ is the estimate of $\mathbf{A}_h$ and is constructed from the estimated values of location and bistatic velocity. For K targets with different location and bistatic velocity, $K!$ candidates of $\hat{\mathbf{A}}_h$ are considered. The main advantage of this method is that the correct combination is determined for all K targets simultaneously. The minimisation in (51) can be interpreted as a maximum likelihood approach due to the AWGN assumption [28].

Remark. *So far it has been assumed that all K targets have different locations and bistatic velocities, hence only $K!$ candidates are considered in the LS-based pair-matching method. While the CC-based method allows repetition in both the location and Doppler domains, it is in fact forced to do so by the nature of its minimisation that is repeated K times, and there is no theoretical criterion to eliminate any of the combinations after processing each target. On the other hand, using the LS-based method repetition may only occur in the Doppler domain since the targets will in reality be located at different 2D locations. Therefore, in order to generalise this proposed method, $K!$ can be treated as the lower bound on the number of possible candidates of $\hat{\mathbf{A}}_h$ and, in an extreme case, when some targets share the exact bistatic velocity, up to K^K candidates may need to be considered. In such case, the computational cost may be noted as a disadvantage when using this method.*

IV. Simulation Results

In order to evaluate the success of the proposed GS-based solution in processing multistatic automotive radar signals and convey its advantage over the state-of-art, computer simulations were run using MATLAB and the CVX package. The radar settings used are shown in Table I.

Table I
Radar Settings Used in the Simulations

Parameter	Value	Parameter	Value
P_t	10 dBm	f_s	5 MHz
G_t	23 dBi	T_c	30 μs
G_r	16 dBi	T	35 μs
σ	0 dBsm	N	150
B	150 MHz	M	128
f_0	77 GHz	L	8
SNR_i	$100-160$ dB	d	1.948 mm

For parameter estimation, the root-mean-square error (RMSE) is used as the performance metric. The MUSIC method is used as the baseline for comparison due to its super-resolution capability and its ability to use the same search grids generated for the GS-based method. The performance metric was measured in two different settings: varying input signal-to-noise ratio (SNR_i) and varying number of processed pulses/snapshots. Note that the SNR_i, defined as

$$SNR_i = \frac{P_t G_t}{P_n}, \tag{52}$$

where P_n is the noise power at the receiver, is used here as opposed to the conventional output SNR defined at the receiver. Following this approach is more suitable when the received signal is a superposition of signals from multiple targets with different ranges. To illustrate this, the output SNR can be defined as

$$SNR_o = \frac{P_t G_t G_r \sigma c^2}{(4\pi)^3 f_0^2 R_{Tx}^2 R_{Rx}^2 P_n} = \frac{G_r \sigma c^2}{(4\pi)^3 f_0^2 R_{Tx}^2 R_{Rx}^2} SNR_i, \tag{53}$$

where R_{Tx} is the transmitter-to-target range and R_{Rx} is the target-to-receiver range. Suppose a target has $R_{Tx} = R_{Rx} = 50$ m, then using the radar settings in Table 1 with $SNR_i = 150$ dB, the equivalent SNR_o is 16.88 dB. However, for another target with $R_{Tx} = R_{Rx} = 40$ m, then $SNR_o = 20.75$ dB. Therefore, demonstrating the performance metrics against SNR_i is more convenient as targets may have different SNR_o. For parameter association, both proposed methods are compared using the probability defined as the ratio between the number of successful pairings and the total number of trials. The performance metric was measured in three different settings: varying SNR_i, varying estimation error, and varying number of targets.

Consider a scenario where two roadside sensors are employed ($H = 2$), one on each side of a smart highway (see Fig. 1). For location estimation, the rectangular search grid is generated such that $(x_1, y_1) = (-4, 55)$ and $(x_I, y_J) = (6, 65)$ with $I = J = 21$. For Doppler estimation, $v_{\min} = 25$ and $v_{\max} = 35$ are considered with $G_d = 128$. The known polar coordinates of the roadside sensors are $[(30.00, -7.66), (30.33, 11.41)]$ and the velocity of the sensing vehicle is $v = 25$.

For the sake of clarity, the methods being compared are described as follows.

- GS-Joint estimates the 2D location $(x, k)_k$ from all H received signals simultaneously in line with Algorithm 1.
- GS-Average estimates the bistatic velocity $v_{h,k}$ from each h-th received signal separately in line with Algorithm 1. Assuming perfect parameter association, the target velocity v_k is then calculated followed by averaging.
- MUSIC-Average estimates 2D location $(x, k)_k$ and bistatic velocity $v_{h,k}$ from each of the H received signals separately using MUSIC. Its implementation follows the same steps as Algorithm 1 with Step 5 being replaced by estimating the location-MUSIC spectrum using $\mathbf{P}_{\mathbf{g},h}$, and Step 11 being replaced by estimating the Doppler-MUSIC spectrum using $\mathbf{V}_{\mathbf{g},h}$. Assuming perfect parameter association, the target velocity v_k is then calculated followed by averaging.
- Pair-CC-ESPRIT pairs the location and bistatic velocity parameters in line with the method in Section III-D.
- Pair-LS pairs the location and bistatic velocity parameters in line with the method in Section III-E.

In Fig. 5 the result of 2D localisation is shown for a scenario with four evenly spaced targets at $SNR_i = 150$ dB with 8 processed pulses. It can be seen that the MUSIC-based method fails to detect two of the targets with the location of the detected ones clearly smeared. On the contrary, the GS-based method results in sharp detected peaks. In Fig. 6 the estimated bistatic velocity spectrum from 16 processed snapshots for this scenario is shown. The GS-based method clearly yields a better result. The running time for the MUSIC-based method is 1.56 seconds and that of the proposed method is 40.17 seconds. The computer used is powered by an 11th Gen Intel(R) Core(TM) i5-1145G7 chip (2.60 GHz base frequency) and carries 8.00 GB of RAM. Note that the time taken by the proposed method could be significantly reduced if we use a dedicated GS-based algorithm instead of the existing convex optimisation toolbox.

A. Comparison of RMSE for Parameter Estimation

1000 Monte Carlo trials are carried out to compute the RMSE performance. In each trial, a different realisation of the noise signal $\mathbf{W}_h$ is generated. One point-like target is placed in the visible region of the sensing vehicle ($K = 1$), and its parameters $(x, y)_k$ and $v_{h,k}$ are drawn from a uniform distribution bounded by two adjacent grid points from their corresponding search grids.

Firstly, the numbers of pulses and snapshots processed for location and Doppler estimation are chosen as 8 and 16, respectively, and SNR_i is varied. The results are shown in Fig. 7. It is evident that GS-Joint outperforms MUSIC-Average at all levels of SNR_i in both location and Doppler estimation.

Next, the number of processed pulses for location estimation is varied between 2 and 8, and the number of processed snapshots for Doppler estimation is varied between 4 and 16, with SNR_i being fixed at 150 dB. The results are shown

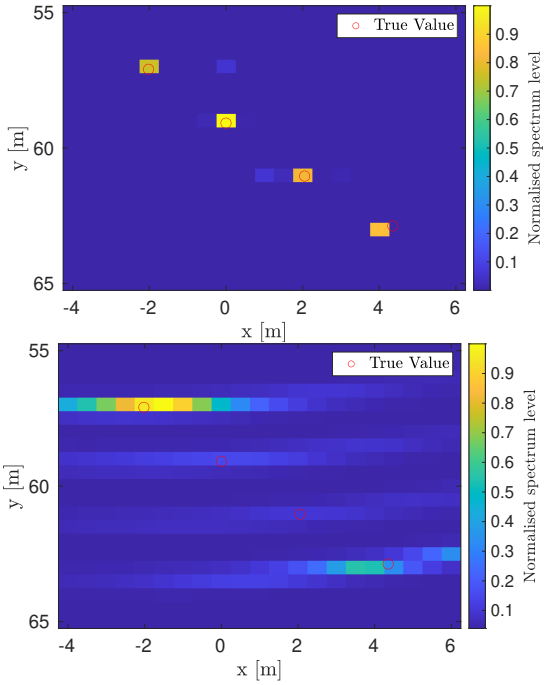

Figure 5. A comparison of a 2D location map computed using GS (top) and MUSIC (bottom) for 4 point targets at $SNR_i = 150$ dB with 8 processed pulses.

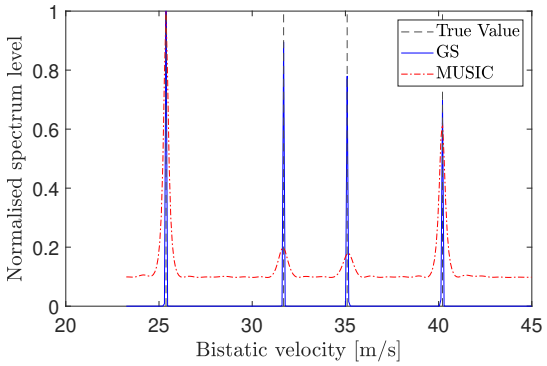

Figure 6. A comparison of a bistatic velocity spectrum computed for 4 point targets at $SNR_i = 150$ dB with 16 processed snapshots.

in Fig. 8. As the number of pulses/snapshots increases, the estimation performance of the proposed method is improved. For all parameters being evaluated, the GS-based method outperforms MUSIC.

B. Comparison of the Probability for Parameter Association

In each trial, the estimated target location and velocity to be used in the pairing methods is randomly selected from a Gaussian distribution with the mean being the true value and the standard deviation σ_e ranging from 0 to 0.5. A different realisation of $\mathbf{W}_h$ is generated in each trial and data from only one roadside sensor is considered.

Firstly, two targets are considered with varied SNR_i. The results are shown in Fig. 9. Pair-LS clearly outperforms Pair-CC-ESPRIT with the latter performing similarly only when SNR_i is above 150 dB and σ_e is below 0.1.

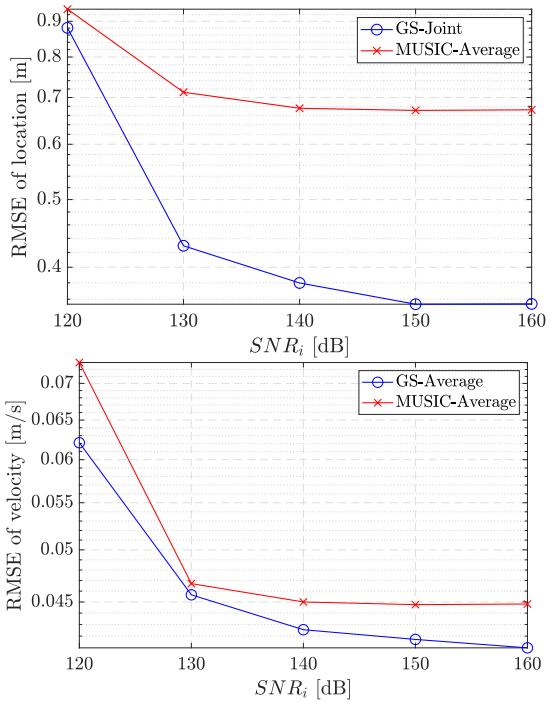

Figure 7. A comparison of RMSE for location (top) and velocity (bottom) estimation between GS and MUSIC against different levels of SNR_i.

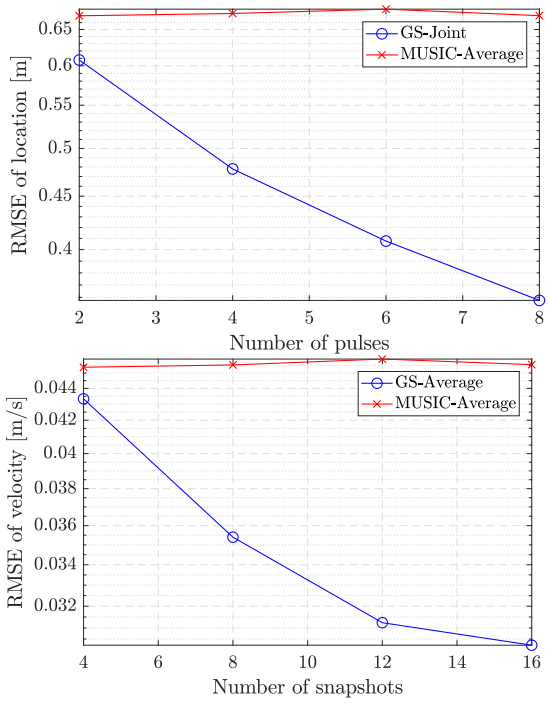

Figure 8. A comparison of RMSE for location (top) and velocity (bottom) estimation between GS and MUSIC as the number of processed pulses/snapshots increases ($SNR_i = 150$ dB).

Next, the number of targets is varied and the SNR_i is fixed at 160 dB. The results are shown in Fig. 10. Again, Pair-LS clearly outperforms Pair-CC-ESPRIT with the latter performing similarly only when $K = 2$ and $\sigma_e \leq 0.1$.

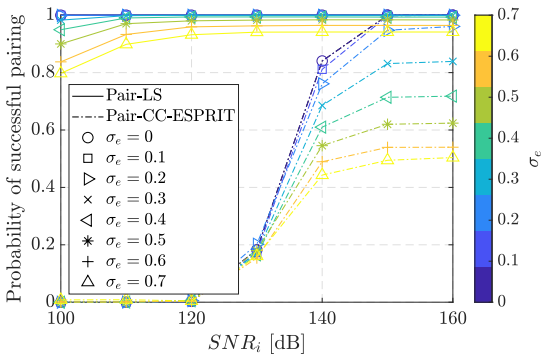

Figure 9. A comparison of the probability of successful pairing between Pair-LS and Pair-CC-ESPRIT against different levels of SNR_i ($K = 2$).

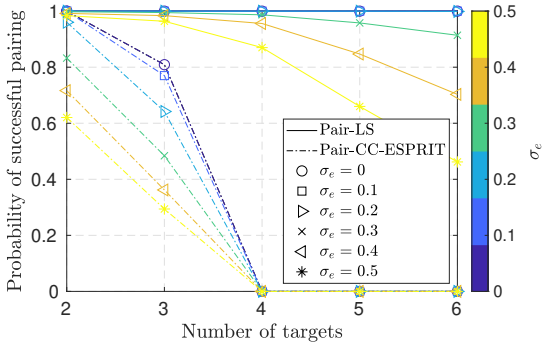

Figure 10. A comparison of the probability of successful pairing between Pair-LS and Pair-CC-ESPRIT as the number of targets increases ($SNR_i = 160$ dB).

V. Conclusion

In this paper, a sparsity-based approach for multistatic automotive localisation was derived. The need for fusing information from multiple sources at the data level was emphasised. The current state-of-art estimation techniques used in the automotive radar industry fail to fulfil such requirements. By employing the GS concept, a method for target location and Doppler estimation was proposed which increases the DoFs and allows information fusion at the data level. Since the natural solution for this application leads to decoupled localisation followed by Doppler estimation, two methods for parameter association were proposed: one relies on the CC between the antenna and pulse domains to match the DOA and bistatic velocity parameters; and the other relies on the whole signal to pair the location and bistatic velocity parameters for all targets simultaneously in an LS-based approach. Computer simulations were conducted to evaluate the performance and verify the effectiveness of the proposed methods. It was shown that GS-based parameter estimation clearly outperforms MUSIC under different settings. The pairing methods also showed evident success in data association under different settings. Bearing the computational cost associated with GS-based optimisation and the LS-based parameter association approach, their attractive performance encourages more research in such advanced signal processing techniques. Accordingly, ways for decreasing the computational complexity will be explored in future work while extending this problem to the four-dimensional wideband case with more extreme traffic scenarios.

References

[1] J. Hasch, E. Topak, R. Schnabel, T. Zwick, R. Weigel, and C. Waldschmidt, "Millimeter-wave technology for automotive radar sensors in the 77 GHz frequency band," *IEEE Transactions on Microwave Theory and Techniques*, vol. 60, no. 3, pp. 845–860, Mar. 2012.

[2] S. Kuutti, S. Fallah, K. Katsaros, M. Dianati, F. Mccullough, and A. Mouzakitis, "A survey of the state-of-the-art localization techniques and their potentials for autonomous vehicle applications," *IEEE Internet of Things Journal*, vol. 5, no. 2, pp. 829–846, Apr. 2018.

[3] S. Sun, A. P. Petropulu, and H. V. Poor, "MIMO radar for advanced driver-assistance systems and autonomous driving: Advantages and challenges," *IEEE Signal Processing Magazine*, vol. 37, no. 4, pp. 98–117, Jul. 2020.

[4] F. Engels, P. Heidenreich, M. Wintermantel, L. Stäcker, M. Al Kadi, and A. M. Zoubir, "Automotive radar signal processing: Research directions and practical challenges," *IEEE Journal of Selected Topics in Signal Processing*, vol. 15, no. 4, pp. 865–878, Mar. 2021.

[5] A. Eskandarian, *Handbook of Intelligent Vehicles*. Springer Nature, 2012.

[6] J. Dickmann, J. Klappstein, M. Hahn, N. Appenrodt, H. L. Bloecher, K. Werber, and A. Sailer, "Automotive radar the key technology for autonomous driving: From detection and ranging to environmental understanding," in *IEEE Radar Conference (RadarConf)*, May 2016, pp. 1–6.

[7] S. M. Patole, M. Torlak, D. Wang, and M. Ali, "Automotive radars: A review of signal processing techniques," *IEEE Signal Processing Magazine*, vol. 34, no. 2, pp. 22–35, Mar. 2017.

[8] P. E. Howland, H. D. Griffiths, and C. J. Baker, "Passive bistatic radar systems," *in Bistatic Radar: Emerging Technology*, pp. 247–313, 2008.

[9] H. D. Griffiths and C. J. Baker, *An Introduction to Passive Radar*. Artech House, 2017.

[10] E. Fishler, A. Haimovich, R. Blum, D. Chizhik, L. Cimini, and R. Valenzuela, "MIMO radar: An idea whose time has come," in *Proceedings of the 2004 IEEE Radar Conference*, April 2004, pp. 71–78.

[11] M. E. Davis, *Advances in Bistatic Radar*. SciTech Publishing, 2007, vol. 2.

[12] J. M. Thomas, C. J. Baker, and H. D. Griffiths, "HF passive bistatic radar potential and applications for remote sensing," in *2008 New Trends for Environmental Monitoring Using Passive Systems*, 2008, pp. 1–5.

[13] L. Gürel, H. Bağcı, J. C. Castelli, A. Cheraly, and F. Tardivel, "Validation through comparison: Measurement and calculation of the bistatic radar cross section of a stealth target," *Radio Science*, vol. 38, no. 3, pp. 1046–1057, 2003.

[14] H. C. Zeng, P. B. Wang, J. Chen, W. Liu, L. L. Ge, and W. Yang, "A novel general imaging formation algorithm for GNSS-based bistatic sar," *Sensors*, vol. 16, no. 3, p. 294, 2016.

[15] H. Griffiths and C. Baker, "Passive coherent location radar systems. part 1: Performance prediction," *IEE Proceedings-Radar, Sonar and Navigation*, vol. 152, no. 3, pp. 153–159, 2005.

[16] Y. D. Zhang, M. G. Amin, and B. Himed, "Structure-aware sparse reconstruction and applications to passive multistatic radar," *IEEE Aerospace and Electronic Systems Magazine*, vol. 32, no. 2, pp. 68–78, Feb. 2017.

[17] N. J. Willis, *Bistatic Radar*. SciTech Publishing, 2005, vol. 2.

[18] H. Wymeersch, G. Seco Granados, G. Destino, D. Dardari, and F. Tufvesson, "5G mmWave positioning for vehicular networks," *IEEE Wireless Communications*, vol. 24, no. 6, pp. 80–86, 2017.

[19] F. Liu, C. Masouros, A. P. Petropulu, H. Griffiths, and L. Hanzo, "Joint radar and communication design: Applications, state-of-the-art, and the road ahead," *IEEE Transactions on Communications*, vol. 68, no. 6, pp. 3834–3862, 2020.

[20] M. Ash, M. Ritchie, K. Chetty, and P. V. Brennan, "A new multistatic FMCW radar architecture by over-the-air deramping," *IEEE Sensors Journal*, vol. 15, no. 12, pp. 7045–7053, 2015.

[21] O. Bar-Shalom, N. Dvorecki, L. Banin, and Y. Amizur, "Accurate time synchronization for automotive cooperative radar (CoRD) applications," in *IEEE International Radar Conference*, 2020, pp. 500–505.

[22] P. J. Beasley and M. A. Ritchie, "Multistatic radar synchronisation using COTS GPS disciplined oscillators," in *International Conference on Radar Systems (RADAR 2022)*, 2022, pp. 429–434.

[23] S. H. Dokhanchi, B. S. Mysore, K. V. Mishra, and B. Ottersten, "A mmWave automotive joint radar-communications system," *IEEE Transactions on Aerospace and Electronic Systems*, vol. 55, no. 3, pp. 1241–1260, 2019.

[24] A. Moussa and W. Liu, "Enhanced detection in automotive applications using bistatic radar with cooperative roadside sensors," in *2021 CIE International Conference on Radar (Radar)*, 2021, pp. 1649–1653.

[25] ——, "A two-stage sparsity-based method for location and doppler estimation in bistatic automotive radar," in *Proc. IEEE Statistical Signal Processing Workshop (SSP)*, 2023, pp. 487–491.

[26] X. Zhang, F. Wang, and H. Li, "An efficient method for cooperative multi-target localization in automotive radar," *IEEE Signal Processing Letters*, vol. 29, pp. 16–20, 2021.

[27] H. J. Nussbaumer, "The fast Fourier transform," in *Fast Fourier Transform and Convolution Algorithms*. Springer, 1981, pp. 80–111.

[28] P. Stoica and R. L. Moses, *Spectral Analysis of Signals*. Pearson Prentice Hall, 2005.

[29] V. Chernyak, "Fundamentals of multisite radar systems," in *Multistatic radars and Multiradar Systems*. Gordon and Breach Science Publishers, 1998.

[30] R. Schmidt, "Multiple emitter location and signal parameter estimation," *IEEE Transactions on Antennas and Propagation*, vol. 34, pp. 276–280, March 1986.

[31] E. J. Candès *et al.*, "Compressive sampling," in *Proceedings of the International Congress of Mathematicians*, vol. 3, 2006, pp. 1433–1452.

[32] J. Odendaal, E. Barnard, and C. Pistorius, "Two-dimensional superresolution radar imaging using the MUSIC algorithm," *IEEE Transactions on Antennas and Propagation*, vol. 42, no. 10, pp. 1386–1391, 1994.

[33] H. Krim and M. Viberg, "Two decades of array signal processing research: The parametric approach," *IEEE Signal Processing Magazine*, vol. 13, no. 4, pp. 67–94, 1996.

[34] M. A. Herman and T. Strohmer, "High-resolution radar via compressed sensing," *IEEE transactions on signal processing*, vol. 57, no. 6, pp. 2275–2284, 2009.

[35] S. Qin, Y. D. Zhang, and M. G. Amin, "Generalized coprime array configurations for direction-of-arrival estimation," *IEEE Transactions on Signal Processing*, vol. 63, no. 6, pp. 1377–1390, March 2015.

[36] Q. Shen, W. Liu, W. Cui, S. Wu, Y. D. Zhang, and M. G. Amin, "Low-complexity direction-of-arrival estimation based on wideband coprime arrays," *IEEE/ACM Transactions on Audio, Speech, and Language Processing*, vol. 23, no. 9, pp. 1445–1456, Sep. 2015.

[37] Q. Shen, W. Liu, W. Cui, and S. L. Wu, "Underdetermined DOA estimation under the compressive sensing framework: A review," *IEEE Access*, vol. 4, pp. 8865–8878, 2016.

[38] S. Sun and Y. D. Zhang, "4D automotive radar sensing for autonomous vehicles: A sparsity-oriented approach," *IEEE Journal of Selected Topics in Signal Processing*, vol. 15, no. 4, pp. 879–891, June 2021.

[39] M. Yuan and Y. Lin, "Model selection and estimation in regression with grouped variables," *Journal of the Royal Statistical Society Series B: Statistical Methodology*, vol. 68, no. 1, pp. 49–67, 2006.

[40] N. Simon, J. Friedman, T. Hastie, and R. Tibshirani, "A sparse-group lasso," *Journal of Computational and Graphical Statistics*, vol. 22, no. 2, pp. 231–245, 2013.

[41] S. Ji, D. Dunson, and L. Carin, "Multitask compressive sensing," *IEEE Transactions on Signal Processing*, vol. 57, no. 1, pp. 92–106, 2009.

[42] Z. Zhang and B. D. Rao, "Extension of SBL algorithms for the recovery of block sparse signals with intra-block correlation," *IEEE Transactions on Signal Processing*, vol. 61, no. 8, pp. 2009–2015, 2013.

[43] Q. Wu, Y. D. Zhang, M. G. Amin, and B. Himed, "Complex multitask Bayesian compressive sensing," in *Proceedings of IEEE International Conference on Acoustics, Speech and Signal Processing*, May 2014, pp. 3375–3379.

[44] Q. Shen, W. Liu, L. Wang, and Y. Liu, "Group sparsity based localization for far-field and near-field sources based on distributed sensor array networks," *IEEE Transactions on Signal Processing*, vol. 68, pp. 6493–6508, 2020.

[45] C. Y. Chen and P. P. Vaidyanathan, "MIMO radar ambiguity properties and optimization using frequency-hopping waveforms," *IEEE Transactions on Signal Processing*, vol. 56, no. 12, pp. 5926–5936, 2008.

[46] H. L. Van Trees, *Optimum Array Processing: Part IV of Detection, Estimation, and Modulation Theory*. John Wiley & Sons, 2002.

[47] F. Colone, D. O'hagan, P. Lombardo, and C. Baker, "A multistage processing algorithm for disturbance removal and target detection in passive bistatic radar," *IEEE Transactions on Aerospace and Electronic Systems*, vol. 45, no. 2, pp. 698–722, 2009.

[48] J. E. Palmer and S. J. Searle, "Evaluation of adaptive filter algorithms for clutter cancellation in passive bistatic radar," in *2012 IEEE Radar Conference*, 2012, pp. 493–498.

[49] J. L. Garry, G. E. Smith, and C. J. Baker, "Direct signal suppression schemes for passive radar," in *2015 Signal Processing Symposium (SPSympo)*, 2015, pp. 1–5.

[50] G. Hakobyan and B. Yang, "High-performance automotive radar: A review of signal processing algorithms and modulation schemes," *IEEE Signal Processing Magazine*, vol. 36, no. 5, pp. 32–44, 2019.

[51] D. Malioutov, M. Cetin, and A. S. Willsky, "A sparse signal reconstruction perspective for source localization with sensor arrays," *IEEE transactions on signal processing*, vol. 53, no. 8, pp. 3010–3022, 2005.

[52] C. Steffens, M. Pesavento, and M. E. Pfetsch, "A compact formulation for the $\ell_{2,1}$ mixed-norm minimization problem," *IEEE Transactions on Signal Processing*, vol. 66, no. 6, pp. 1483–1497, 2018.

[53] S. Kikuchi, H. Tsuji, and A. Sano, "Pair-matching method for estimating 2-D angle of arrival with a cross-correlation matrix," *IEEE Antennas and Wireless Propagation Letters*, vol. 5, pp. 35–40, 2006.

[54] R. Roy and T. Kailath, "ESPRIT-estimation of signal parameters via rotational invariance techniques," *IEEE Transactions on Acoustics, Speech, and Signal Processing*, vol. 37, no. 7, pp. 984–995, 1989.

[55] G. Lu and W. Ping, "Comments on 'Pair-matching method for estimating 2-D angle of arrival with a cross-correlation matrix'," *IEEE Antennas and Wireless Propagation Letters*, vol. 7, p. 807, 2008.